Extensive L^2 calculation of partial photoionization cross sections of He in the $4lnl'$ resonance region

I. Sánchez and F. Martín
Departamento de Química C-14, Universidad Autónoma de Madrid, 28049-Madrid, Spain
(Received 25 March 1993)

We present a fully-L^2-integrable calculation of the partial photoionization cross sections of He between the $N=3$ and 4 thresholds. The energy positions, total and partial autoionization widths, and Fano and Starace parameters for the $4lnl'$ doubly excited states lying in this region are also provided. We have found that only one series of resonances with large autoionization widths is observed in the total-cross-section spectrum. On the other hand, several resonance series are exhibited in the partial $N=3$ cross sections. Our results also show that the $2p$ and $3p$ cross sections dominate the $N=2$ and 3 ones, respectively. Good agreement with the existing experimental data is found.

PACS number(s): 32.80.Fb, 32.80.Dz, 31.50.+w

I. INTRODUCTION

Photoionization of the helium atom from the ground state is a subject of growing interest, since it is essential to understand the role of electron correlation in continuum states. In particular, the $^1P^\circ$ doubly excited states lying above the ionization threshold are selectively populated in these experiments, so that resonance parameters can be determined with high accuracy. Most experimental and theoretical works have been devoted to study photoionization below the $N=3$ threshold, and to characterize the $2lnl'$ and $3lnl'$ doubly excited states of He. In the last years, a deeper insight has been obtained from the analysis of partial photoionization cross sections (see for instance Refs. [1–13]).

Theoretical studies above the $N=3$ threshold including resonance structure are very scarce. The only calculations of photoionization cross sections of helium between the $N=3$ and 4 thresholds that we are aware of have been recently reported by Hayes and Scott [8] and Martín [14]. The first one is based on the R-matrix method and has given $N=2$ and 3 partial cross sections, as well as the $3s$, $3p$, and $3d$ contributions to the latter. Calculations of Martín have been performed with an L^2-integrable method based on the Feshbach formalism and have provided $N=1$, 2, and 3 partial cross sections. None of these previous works has reported partial cross sections for each individual open channel. Also, a detailed analysis of the resonance structures observed in the cross-section spectra is lacking. Although there are some theoretical works that have provided energy positions and total autoionization widths for the $4lnl'$ doubly excited states lying between the $N=3$ and 4 thresholds [15–20], nothing is known about partial autoionization widths or Fano and Starace parameters.

From the experimental side, Woodruff and Samson [3] have measured the total photoionization cross sections for leaving the He^+ ion in an excited state ($\sigma_{N=2}+\sigma_{N=3}$) as a function of the photon energy, and Heimann *et al.* [21] have been able to separate the $N=3$ contribution at four different energies. More recently, Domke *et al.* [22] have obtained the spectrum for the total photoionization cross section with high-energy resolution, and Zubek *et al.* [5] have measured the $N=2$ differential cross section at 90°.

In this paper we present extensive calculations of partial photoionization cross sections and $4lnl'$ resonance parameters of He between the $N=3$ and 4 thresholds. For this purpose we use the L^2 method recently proposed by Martín ([14], hereafter called paper I), which takes into account (strong) interchannel coupling in a fully algebraic way. This method is well adapted to obtain accurate representations of the resonance structures observed in the cross-section spectra, and therefore can be used to obtain energy positions, total and partial autoionization widths, and Fano and Starace parameters.

The paper is organized as follows. The theoretical method is briefly outlined in Sec. II. A detailed explana-

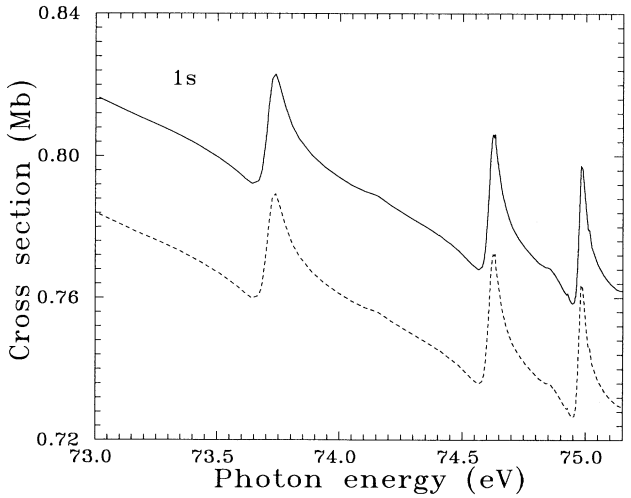

FIG. 1. Partial σ_{1s} photoionization cross section of helium above the $N=3$ threshold. ——, length gauge; — — —, velocity gauge.

tion can be found in paper I. In Sec. III, we present and discuss our results for cross sections and resonance parameters. Comparison with previous works is done when it is possible. We end the paper with some conclusions in Sec. IV. Atomic units are used throughout the paper unless otherwise stated.

II. THEORETICAL METHOD

The ground-state wave function of helium is the same used in paper I and in Refs. [11–13]. There are nine open channels above $N=3$: $\mu=1s\varepsilon p$, $2s\varepsilon p$, $2p\varepsilon s$, $2p\varepsilon d$, $3s\varepsilon p$, $3p\varepsilon s$, $3p\varepsilon d$, $3d\varepsilon p$, and $3d\varepsilon f$. For each channel μ, the exact continuum wave function $\psi^{-}_{\mu E}$ is written as [12]

$$|\psi^{-}_{\mu E}\rangle=\frac{\langle\phi_s|Q\mathcal{H}P|P\psi^{0-}_{\mu E}\rangle}{E-\mathcal{E}_s-\Delta_s(E)-i[\Gamma_s(E)/2]}|\phi_s\rangle$$
$$+[1+G^{(s)}_Q(E)Q\mathcal{H}P]\left[|P\psi^{0-}_{\mu E}\rangle+\frac{\langle\phi_s|Q\mathcal{H}P|P\psi^{0-}_{\mu E}\rangle}{E-\mathcal{E}_s-\Delta_s(E)-i[\Gamma_s(E)/2]}G^{(s)-}_P(E)P\mathcal{H}Q|\phi_s\rangle\right], \quad (1)$$

where P is a two-electron projection operator of the form [23]:

$$P=P_1+P_2-P_1P_2\ , \quad (2)$$

with

$$P_i=\sum_{N=1}^{3}\sum_{l=0}^{N-1}\sum_{m=-1}^{l}|\varphi_{Nlm}(i)\rangle\langle\varphi_{Nlm}(i)|\ , \quad (3)$$

which includes all hydrogenic φ_{Nlm} states of He^+ with $N\leq 3$, ϕ_s is a resonant wave function of energy $\mathcal{E}_s$, which is the solution of a projected Schrödinger equation in the Q subspace, $G^{(s)}_Q(E)$ in the Green operator in Q subspace in which the s state has been excluded, $P\psi^{0-}_{\mu E}$ is a nonresonant wave function of energy E which is the eigenstate of $P\mathcal{H}P+P\mathcal{H}QG^{(s)}_Q(E)Q\mathcal{H}P$, $G^{(s)-}_P(E)$ is the corresponding Green operator in P subspace, $\Gamma_s(E)$ is the "width," and $\Delta_s(E)$ is the "shift" of the ϕ_s resonance at the energy E.

In order to obtain the continuum state of Eq. (1), we need to evaluate two kinds of wave functions, ϕ_n and $P\psi^{0-}_{\mu E}$, and the corresponding Green operators, $G^{(s)}_Q(E)$ and $G^{(s)-}_P(E)$. The ϕ_n wave functions have been evaluated in the framework of the pseudopotential-Feshbach method [24] using the Slater-type-orbital (STO) basis set reported in paper I. The basis of 216 configurations includes STO's from $n=1$ to 8, and angular momenta from $l=0$ to 5, and is accurate enough to represent Feshbach resonances lying below $N=4$. The expansion of $G^{(s)}_Q(E)$ includes the first 43 eigenfunctions of $Q\mathcal{H}Q$ that represent $nln'l'$ doubly excited states with $n,n'\geq 4$, and discretized $nl\varepsilon l'$ continuum functions with $n=4$ that our basis is able to reproduce up to the $N=5$ threshold.

The Green function $G^{(s)-}_P(E)$ is obtained in a basis of L^2 uncoupled states $\tilde{\chi}^0_{\mu n}$ by solving the system of linear equations [14]:

$$\sum_{\mu'',n''}\mathcal{C}_{\mu'n'\mu''n''}\langle\tilde{\chi}^0_{\mu''n''}|G^{(s)-}_P(E)|\tilde{\chi}^0_{\mu n}\rangle=\mathcal{D}_{\mu'n'}\ , \quad (4)$$

where the coefficients $\mathcal{C}_{\mu'n'\mu''n''}$ and $\mathcal{D}_{\mu'n'}$ are given by

$$\mathcal{C}_{\mu'n'\mu''n''}=\delta_{\mu''\mu'}\delta_{n''n'}-\Xi_{\mu'}(E_{n'})\langle\tilde{\chi}^0_{\mu'n'}|V|\tilde{\chi}^0_{\mu''n''}\rangle\ , \quad (5)$$

$$\mathcal{D}_{\mu'n'}=\delta_{\mu'\mu}\delta_{n'n}\Xi_{\mu'}(E_{n'})\ . \quad (6)$$

In Eqs. (4)–(6), $\{\tilde{\chi}^0_{\mu n}\}$ is a complete set of L^2 orthogonal uncoupled-continuum-wave functions, which are solu-

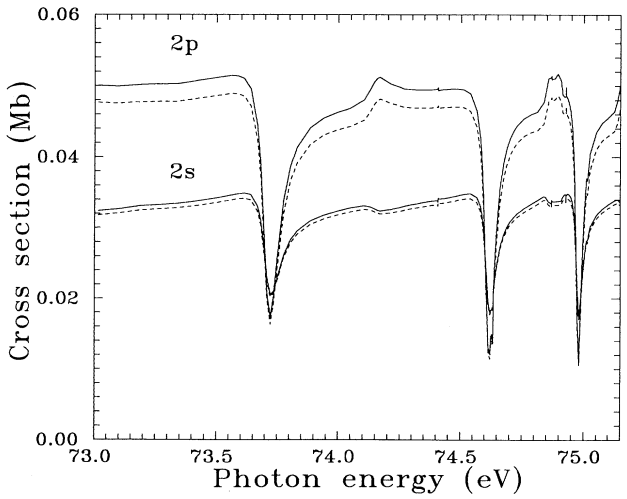

FIG. 2. Partial σ_{2s} and σ_{2p} photoionization cross sections of helium above the $N=3$ threshold. ——, length gauge, — — —, velocity gauge.

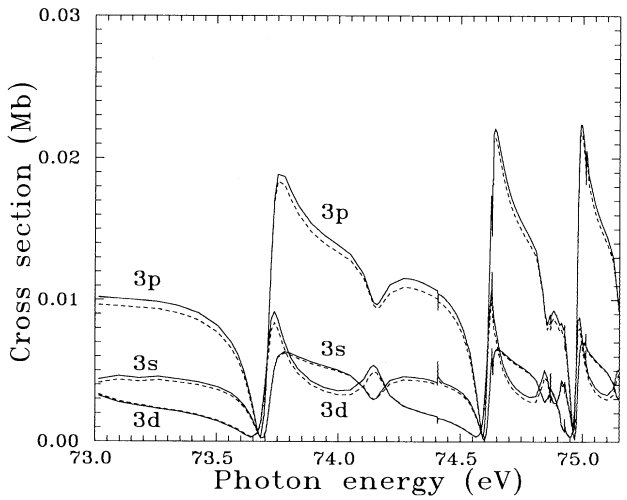

FIG. 3. Partial σ_{3s}, σ_{3p}, and σ_{3d} photoionization cross sections of helium above the $N=3$ threshold. ——, length gauge; — — —, velocity gauge.

tions of single-channel Schrödinger equations, V is the interaction potential that includes the interchannel couplings and the polarization potential [12], and

$$\Xi_{\mu'}(E_{n'})=\begin{cases} i\pi\rho_{\mu'}(E_{n'}) & \text{for } E_{n'}=E_n \\ 1/(E_n-E_{n'}) & \text{for } E_{n'}\neq E_n \end{cases}, \tag{7}$$

where $\rho_\mu(E_n)$ is the square of the appropriate renormalization factor for the $\tilde{\chi}^0_{\mu n}$ functions to be properly δ normalized. Equation (4) represents a system of linear equations in the complex plane for each channel μ. The coefficient **C** multiplying the unknowns is the same for all μ, so that each system of equations differs exclusively in the right-hand-side column vector **D**. Therefore, only one matrix inversion is required to solve Eqs. (4). The L^2 $\tilde{\chi}^0_{\mu n}$ states are evaluated with an even-tempered basis of (STO's) using the standard computer codes of Macías *et al.* [25], which also provide the renormalization factors $\rho_\mu(E_n)$, for each channel μ and each energy E_n.

Then, the $P\psi^{0-}_{\mu E}$ nonresonant wave function is written as

$$P\psi^{0-}_{\mu En}=\rho^{1/2}_\mu(E_n)\left[\tilde{\chi}^0_{\mu n}+\sum_{\mu',n'}\sum_{\mu'',n''}\langle\tilde{\chi}^0_{\mu''n''}|G^{(s)-}_P(E_n)|\tilde{\chi}^0_{\mu'n'}\rangle\langle\tilde{\chi}^0_{\mu'n'}|V|\tilde{\chi}^0_{\mu n}\rangle\tilde{\chi}^0_{\mu''n''}\right]. \tag{8}$$

The cross sections have been evaluated in the dipole approximation for photon energies between 73.00 and 73.16 eV. An energy grid with variable step size has been used in order to exhibit the whole resonant structure. All calculations have been done in quadruple precision.

III. RESULTS AND DISCUSSION

In Figs. 1–3 we show the $1s$, the $2s$ and $2p$, and the $3s$, $3p$, and $3d$ partial cross sections in both the length and velocity representations. The total cross section is displayed in Fig. 4. Gauge invariance is good for $2s$, $2p$, $3s$, $3p$, and $3d$ cross sections. For the $1s$ one, as well as for the total one, the velocity results are $\sim 5\%$ lower than the length results; however, the corresponding curves are practically parallel. This may be explained by the fact that the $1s\varepsilon p$ continuum has the strongest oscillatory behavior, so that the STO basis used to represent the nonresonant wave function is less complete than for other channels.

The largest contribution to the total cross section comes from the $1s$ one, which means that the He^+ ion is left preferentially in the ground state. The $2p$ cross section dominates over the $2s$ one in the whole energy range considered in Fig. 2. Also, the $3p$ partial cross section is larger than the $3s$ and $3d$ ones.

There are seven series of autoionizing resonances converging to the $N=4$ threshold, namely $(2,1)_n$, $(3,0)_n$, $(0,1)_n$, $(1,0)_n$, $(-1,0)_n$, $(-2,1)_n$, and $(-3,0)_n$. According to Herrick and Sinanoglu [16], we have labeled them using the K and T quantum numbers: $(K,T)_n$. Only one strong series of resonances is observed in Figs. 1–4: the peaks at 73.72, 74.62, and 74.99 eV, which correspond to the first three (2,1) $4lnl'$ doubly excited states. Resonances of other series are practically invisible in the $1s$ and the total cross sections.

In the $2s$ and $2p$ cross sections, one can also distinguish some broad structures at 74.16, 74.86, and 75.16 eV, which correspond to the first three doubly excited states of the (0,1) series. These are much more apparent in the $3s$, $3p$, and $3d$ cross sections shown in Fig. 3. In the latter figure, there are also needlelike peaks at 74.42 and 74.88 eV corresponding to the (3,0) series, and at 74.64 and 75.02 eV corresponding to the (1,0) one. The two latter resonances are embedded in the wider $(2,1)_5$ and $(2,1)_6$ ones. Finally, one can also see a small hump at 74.91 eV

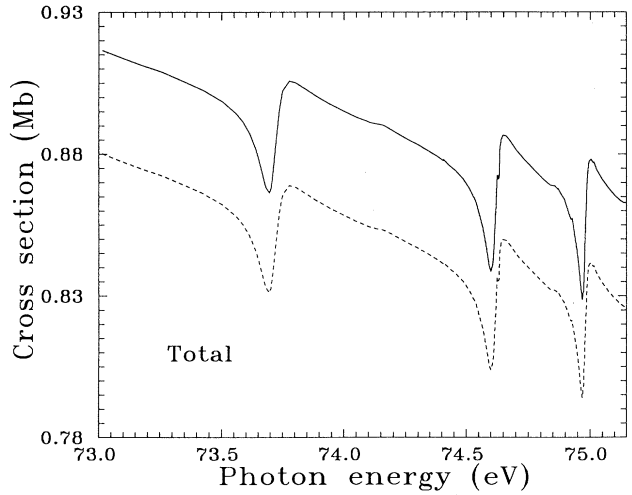

FIG. 4. Total photoionization cross section of helium above the $N=3$ threshold. ——, length gauge; — — —, velocity gauge.

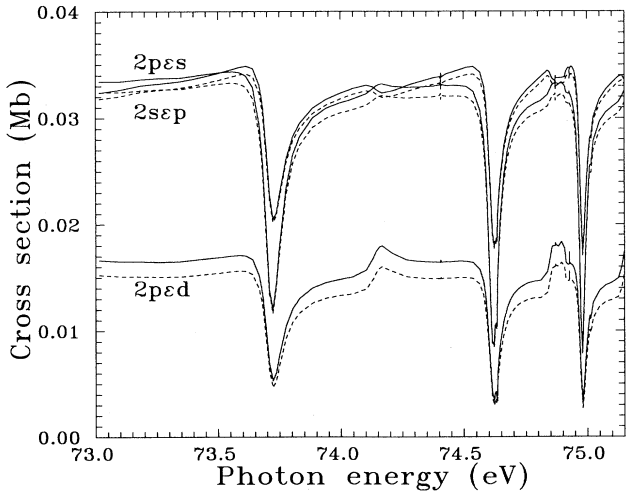

FIG. 5. Partial $\sigma_{2s\varepsilon p}$, $\sigma_{2p\varepsilon s}$, and $\sigma_{2p\varepsilon d}$ photoionization cross sections of helium above the $N=3$ threshold. ——, length gauge; — — —, velocity gauge.

due to the presence of the first $(-2,1)$ resonance, and a small needlelike peak at 74.93 eV which corresponds to the first $(-1,0)$ one. A more detailed description of these doubly excited states is given below by analyzing the resonance parameters.

The $3s$, $3p$, and $3d$ partial cross sections have been also evaluated by Hayes and Scott [8]. The overall agreement with our results is reasonable. However, there are some significant discrepancies: (i) although the $3s$ and $3d$ cross sections are comparable in both calculations, the $3s$ one dominates over the $3d$ one at energies lower than those reported by Hayes and Scott; (ii) in general, our resonance positions are shifted to lower energies; (iii) the needlelike peaks of the $(3,0)_n$ series (wrongly attributed to the $(-2,1)_n$ series in Ref. [8]) are much smaller in the present calculations; and (iv) resonances belonging to the (0,1), $(-2,1)$, and $(-1,0)$ series are not observed in the cross sections reported by Hayes and Scott [8].

We show in Figs. 5 and 6 the $2l\varepsilon l'$ and $3l\varepsilon l'$ partial cross sections. The $2p\varepsilon s$ and $2s\varepsilon p$ cross sections are roughly comparable, and both are larger than the $2p\varepsilon d$ one. In Figs. 6(a) and 6(b) one can see that the $N=3$ partial cross sections approximately follow the ordering $3p\varepsilon s > 3s\varepsilon p > 3p\varepsilon d > 3d\varepsilon p > 3d\varepsilon f$. Also, the needlelike structures are much more visible than in previous plots (see Fig. 3). This is an indication that the addition of partial cross sections can be responsible for the lack of some resonance series in the spectra.

Although comparison with the experimental results was given in paper I, we include it here for completeness.

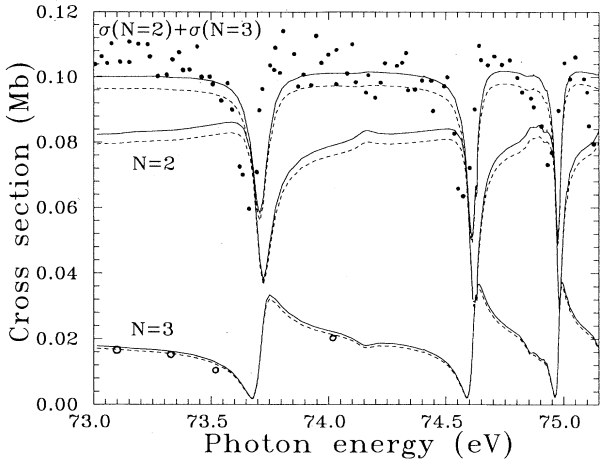

FIG. 7. $\sigma_{N=2}$ and $\sigma_{N=3}$ photoionization cross sections of helium above the $N=3$ threshold. ——, length gauge; — — —, velocity gauge; ●, experimental values of Woodruff and Samson [3]; ○, experimental values of Heimann *et al.* [21].

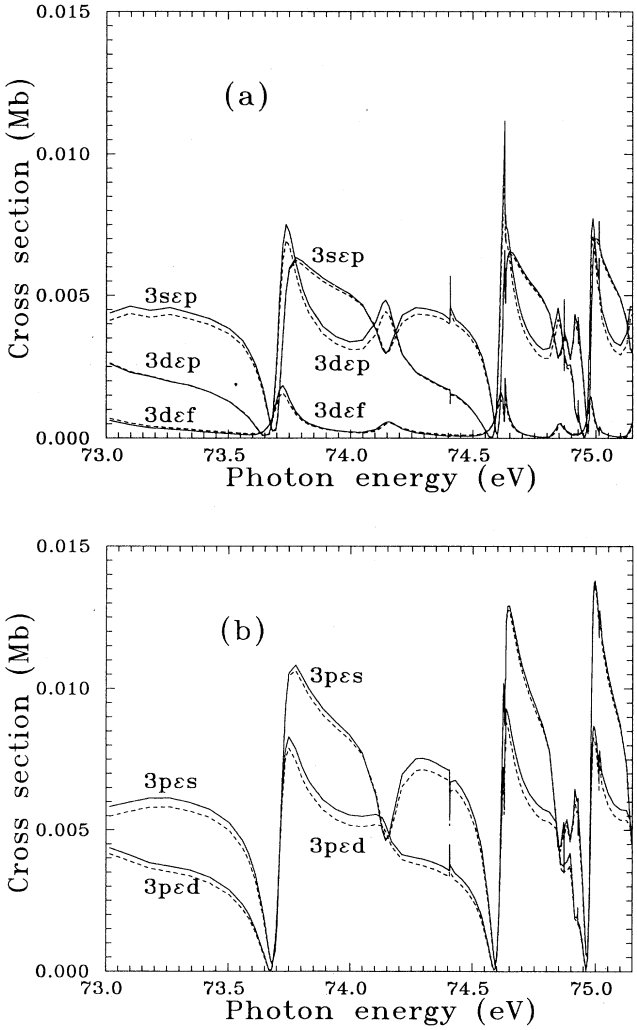

FIG. 6. Partial $\sigma_{3s\varepsilon p}$, $\sigma_{3d\varepsilon p}$, and $\sigma_{3d\varepsilon f}$ (a) and $\sigma_{3p\varepsilon s}$ and $\sigma_{3p\varepsilon d}$ (b) photoionization cross sections of helium above the $N=3$ threshold. ——, length gauge, — — —, velocity gauge.

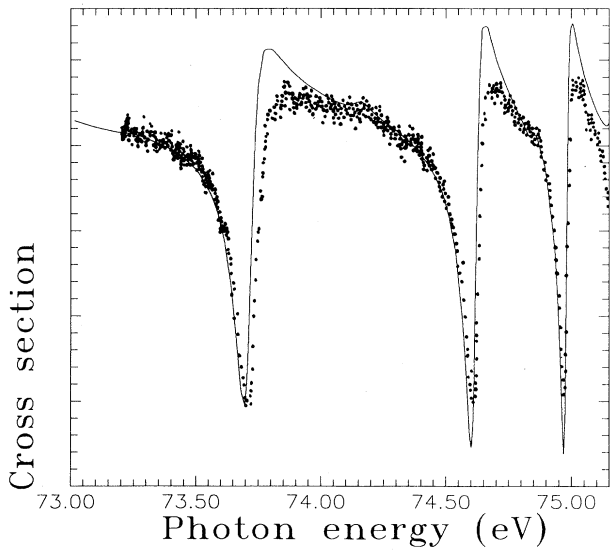

FIG. 8. Total photoionization cross section of helium above the $N=3$ threshold. The background cross section has been substracted from the results of Fig. 4; the experimental cross sections (●) of Domke *et al.* [22] have been normalized to the theoretical values at the first minimum.

In Fig. 7 we have plotted the $N=2$ and 3 cross sections. The latter is compared with the experimental results of Heimann *et al.* [21]. The agreement between experiment and theory is very good. As Woodruff and Samson [3] have measured the $\sigma_{N=2}+\sigma_{N=3}$ cross section between the $N=3$ and 4 thresholds, we also compare in this figure the experimental data with the corresponding theoretical results. The overall agreement is good, although the resonance peaks in the experiment are shifted to lower energies. It can be observed in Fig. 7 that the needlelike peaks that are present in the individual partial cross sections have practically disappeared from the $N=3$ cross section. The same holds for the sum $\sigma_{N=2}+\sigma_{N=3}$.

Very recently, Domke *et al.* [22] have measured, with high-energy resolution, the total photoionization yield in the energy region between 73.2 and 75.5 eV. In this experiment, the cross sections were obtained in arbitrary units. As explained in paper I, comparison can be made by substracting the slow decreasing background from the results of Fig. 4, and by normalizing the experimental data to ours at the first minimum. The resulting comparison is displayed in Fig. 8. The use of the length and the velocity data leads to identical graphs. Both energy positions and shapes of the resonance peaks are in very good agreement. In particular, it can be observed that, in this kind of representation, the first (0,1) resonance at 74.16 eV is more clearly exhibited than in Fig. 4.

Now we analyze in greater detail the resonances observed in the photoionization spectra. As shown by Fano [26], the total cross section can be parametrized in the vicinity of each resonance using the formula

$$\sigma(E)=\sigma^0\left[\rho_s^2\frac{(q_s+\epsilon)^2}{1+\epsilon^2}+1-\rho_s^2\right], \tag{9}$$

where $\epsilon=2[E-\mathcal{E}_s-\Delta_s(\mathcal{E}_s)]/\Gamma_s(\mathcal{E}_s)$, σ^0 is the background nonresonant cross section, q_s is the line profile parameter, and ρ_s^2 is the correlation parameter. The partial cross sections can be parametrized following Starace [27]:

$$\sigma_\mu(E)=\frac{\sigma_\mu^0(E)}{1+\epsilon^2}\{\epsilon^2+2\epsilon[q_s\mathrm{Re}(\alpha_\mu^s)-\mathrm{Im}(\alpha_\mu^s)]+1 -2q_s\mathrm{Im}(\alpha_\mu^s)-2\,\mathrm{Re}(\alpha_\mu^s) +(q_s^2+1)|\alpha_\mu^s|^2\}\,, \tag{10}$$

where σ_μ^0 is the partial background nonresonant cross section and α_μ^s are the Starace parameters. As shown by Sánchez and Martín [12], Eq. (1) leads to Eqs. (9) and (10) in the neighborhood of each resonance s, where all these parameters remain practically constant. Therefore, no fitting procedure is needed to evaluate the resonance parameters, which are directly obtained for $E=\mathcal{E}_s$. The latter take into account the effect of neighboring resonances through the terms including the $G_Q^{(s)}(E)$ operator.

In Tables I and II we present the set of Fano and Starace parameters for the 12 resonances observed between 73.00 and 75.15 eV. Table II also includes the partial autoionization widths. From Table I, one can see that the largest autoionization widths correspond to the resonances of the $(2,1)_n$, $(0,1)_n$, and $(-2,1)_n$ series. In fact, the use of the approximate selection rules proposed by Herrick and Sinanoglu [16] indicates that these are the only resonances for which autoionization is allowed. The correlation parameter ρ_s^2 is very small for all the resonant states except for those of the (2,1) series. As the maximum and the minimum of a resonant peak are approximately equal to $\sigma^0(1+\rho_s^2q_s^2)$ and $\sigma^0(1-\rho_s^2)$, respectively, the previous result explains why only (2,1) resonances are observed in the total-cross-section spectrum. In particular, the (0,1) resonances, which have the largest widths, are practically invisible in the total-cross-section spectrum since ρ_s^2 is of the order of 10^{-3}. Within the (2,1) series, the q_s and ρ_s^2 parameters remain practically constant ($q_s=0.48$, 0.59, and 0.55; $\rho_s^2=0.037$, 0.041, and 0.044). This behavior is less apparent for the remaining series, which have much larger q_s and much smaller ρ_s^2 values. Also, the great closeness between some resonances (the fourth and fifth, the sixth and seventh, and the eighth, ninth, and tenth) implies some aleatory char-

TABLE I. Energy positions, total autoionization widths, and Fano parameters for the $4lnl'$ doubly excited states of He. The energy positions include the Feshbach shift and are referred to the ground-state energy, $E_g=-2.903\,724\,38$ a.u. We have used the equivalence 1 a.u.=27.211 687 eV. The numbers in brackets indicate powers of ten. Each resonance is labeled $k\,{}^1P^\circ(K,T)_n$, where k indicates the energy ordering and n the principal quantum number of the outer electron.

s	$\varepsilon_s+\Delta_s$ (eV)	Γ_s (eV)	ρ_s^2	q_s	σ^0 (Mb)
$1\,{}^1P^\circ(2,1)_4$	73.724 57	0.775 398[−1]	0.371 031[−1]	0.483 458	0.899 539
$2\,{}^1P^\circ(0,1)_4$	74.163 24	0.969 120[−1]	0.147 039[−3]	0.333 609[+1]	0.888 274
$3\,{}^1P^\circ(3,0)_5$	74.420 53	0.105 171[−2]	0.191 881[−5]	−0.145 811[+2]	0.877 678
$4\,{}^1P^\circ(2,1)_5$	74.627 71	0.483 228[−1]	0.416 017[−1]	0.594 079	0.874 839
$5\,{}^1P^\circ(1,0)_5$	74.642 71	0.239 858[−2]	0.109 355[−2]	−0.520 567	0.872 181
$6\,{}^1P^\circ(0,1)_5$	74.863 36	0.361 068[−1]	0.622 678[−3]	0.146 496[+1]	0.868 830
$7\,{}^1P^\circ(3,0)_6$	74.883 87	0.857 783[−3]	0.404 873[−4]	−0.307 124[+1]	0.867 555
$8\,{}^1P^\circ(-2,1)_4$	74.920 10	0.156 171[−1]	0.105 334[−2]	−0.910 440	0.861 081
$9\,{}^1P^\circ(-1,0)_5$	74.941 01	0.232 686[−3]	0.493 249[−5]	0.956 832[+1]	0.856 981
$10\,{}^1P^\circ(2,1)_6$	74.990 08	0.290 813[−1]	0.444 135[−1]	0.552 576	0.866 976
$11\,{}^1P^\circ(1,0)_6$	75.026 70	0.146 368[−2]	0.258 768[−3]	−0.231 638[−2]	0.877 123
$12\,{}^1P^\circ(0,1)_6$	75.162 37	0.257 576[−1]	0.152 355[−3]	0.283 001[+1]	0.862 004

TABLE II. Partial autoionization widths and Starace parameters for the $4lnl'$ doubly excited states of He. Notation as in Table I.

s	μ	σ_μ^0 (Mb)	Γ_μ^s (eV)	Re (α_μ^s)	Im (α_μ^s)
$1\,^1P^\circ(2,1)_4$	$1s\varepsilon p$	0.799 006	0.628 401[−3]	−0.127 754[−2]	−0.183 547[−1]
	$2s\varepsilon p$	0.329 277[−1]	0.353 507[−2]	0.940 305[−1]	0.193 310
	$2p\varepsilon s$	0.327 728[−1]	0.104 982[−1]	0.245 992	0.278 155
	$2p\varepsilon d$	0.158 494[−1]	0.604 617[−2]	0.233 461	0.331 204
	$3s\varepsilon p$	0.477 494[−2]	0.843 769[−2]	0.859 969	−0.145 131
	$3p\varepsilon s$	0.726 817[−2]	0.146 041[−1]	0.899 452	−0.236 362
	$3p\varepsilon d$	0.434 810[−2]	0.136 278[−1]	0.108 610[+1]	−0.411 648
	$3d\varepsilon p$	0.238 274[−2]	0.149 309[−1]	0.146 548[+1]	−0.741 332
	$3d\varepsilon f$	0.209 704[−3]	0.523 134[−2]	0.324 344[+1]	−0.466 706
$2\,^1P^\circ(0,1)_4$	$1s\varepsilon p$	0.787 062	0.279 467[−4]	−0.150 517[−4]	−0.218 239[−3]
	$2s\varepsilon p$	0.330 067[−1]	0.582 025[−3]	−0.400 215[−2]	0.278 354[−2]
	$2p\varepsilon s$	0.323 082[−1]	0.439 845[−3]	0.948 214[−3]	−0.417 720[−2]
	$2p\varepsilon d$	0.156 047[−1]	0.642 367[−2]	0.847 217[−2]	−0.219 776[−1]
	$3s\varepsilon p$	0.491 829[−2]	0.163 050[−1]	0.314 365[−1]	0.589 891[−1]
	$3p\varepsilon s$	0.819 802[−2]	0.327 621[−1]	0.306 988[−1]	0.666 602[−1]
	$3p\varepsilon d$	0.463 536[−2]	0.400 235[−2]	−0.341 097[−1]	0.455 148[−3]
	$3d\varepsilon p$	0.243 589[−2]	0.241 180[−1]	−0.600 735[−1]	−0.986 672[−1]
	$3d\varepsilon f$	0.105 596[−3]	0.122 511[−1]	0.935 170[−1]	−0.384 209
$3\,^1P^\circ(3,0)_5$	$1s\varepsilon p$	0.777 628	0.401 529[−7]	0.893 308[−5]	0.169 784[−5]
	$2s\varepsilon p$	0.339 359[−1]	0.608 371[−5]	−0.531 640[−3]	−0.664 995[−4]
	$2p\varepsilon s$	0.330 063[−1]	0.793 294[−5]	0.619 433[−3]	0.341 434[−4]
	$2p\varepsilon d$	0.164 595[−1]	0.243 181[−5]	−0.386 565[−3]	0.295 210[−3]
	$3s\varepsilon p$	0.426 486[−2]	0.364 313[−3]	−0.741 110[−2]	0.904 768[−2]
	$3p\varepsilon s$	0.702 684[−2]	0.374 825[−3]	0.479 840[−2]	−0.789 879[−2]
	$3p\varepsilon d$	0.360 966[−2]	0.151 474[−3]	−0.383 637[−2]	0.724 418[−2]
	$3d\varepsilon p$	0.165 723[−2]	0.126 927[−3]	−0.722 844[−2]	−0.838 997[−2]
	$3d\varepsilon f$	0.893 108[−4]	0.176 856[−4]	−0.172 968[−1]	−0.423 238[−2]
$4\,^1P^\circ(2,1)_5$	$1s\varepsilon p$	0.774 048	0.483 674[−3]	−0.335 611[−2]	−0.214 326[−1]
	$2s\varepsilon p$	0.335 449[−1]	0.268 677[−2]	0.130 273	0.208 214
	$2p\varepsilon s$	0.322 029[−1]	0.781 485[−2]	0.309 165	0.295 280
	$2p\varepsilon d$	0.156 258[−1]	0.457 885[−2]	0.303 555	0.358 544
	$3s\varepsilon p$	0.487 620[−2]	0.519 248[−2]	0.888 749	−0.110 168
	$3p\varepsilon s$	0.790 032[−2]	0.972 455[−2]	0.938 078	−0.216 978
	$3p\varepsilon d$	0.423 100[−2]	0.730 045[−2]	0.108 169[+1]	−0.359 874
	$3d\varepsilon p$	0.236 419[−2]	0.842 128[−2]	0.143 035[+1]	−0.798 036
	$3d\varepsilon f$	0.453 756[−4]	0.211 994[−2]	0.485 436[+1]	0.340 920[+1]
$5\,^1P^\circ(1,0)_5$	$1s\varepsilon p$	0.806 132	0.540 488[−6]	0.406 396[−3]	−0.318 512[−3]
	$2s\varepsilon p$	0.184 815[−1]	0.342 809[−5]	−0.679 121[−2]	−0.525 711[−2]
	$2p\varepsilon s$	0.104 437[−1]	0.450 648[−5]	−0.547 016[−2]	0.119 021[−1]
	$2p\varepsilon d$	0.404 527[−2]	0.335 596[−4]	0.350 412[−1]	0.455 077[−1]
	$3s\varepsilon p$	0.500 110[−2]	0.306 639[−3]	−0.405 916[−1]	0.150 776
	$3p\varepsilon s$	0.103 645[−1]	0.149 284[−3]	0.532 133[−1]	−0.538 120[−1]
	$3p\varepsilon d$	0.776 694[−2]	0.408 997[−3]	0.353 842[−1]	−0.140 311
	$3d\varepsilon p$	0.858 449[−2]	0.726 395[−3]	0.246 360[−1]	0.181 770
	$3d\varepsilon f$	0.136 151[−2]	0.765 226[−3]	−0.123 235	−0.456 405
$6\,^1P^\circ(0,1)_5$	$1s\varepsilon p$	0.767 832	0.161 256[−4]	0.601 974[−4]	−0.557 718[−3]
	$2s\varepsilon p$	0.337 566[−1]	0.214 874[−3]	−0.911 605[−2]	0.350 321[−2]
	$2p\varepsilon s$	0.322 580[−1]	0.129 438[−3]	0.277 270[−2]	−0.724 116[−2]
	$2p\varepsilon d$	0.159 288[−1]	0.216 188[−2]	0.231 622[−1]	−0.386 920[−1]
	$3s\varepsilon p$	0.429 359[−2]	0.361 311[−2]	0.869 753[−1]	0.710 210[−1]
	$3p\varepsilon s$	0.738 619[−2]	0.968 164[−2]	0.775 419[−1]	0.116 735
	$3p\varepsilon d$	0.486 892[−2]	0.319 258[−2]	−0.538 634[−1]	0.832 072[−1]
	$3d\varepsilon p$	0.246 803[−2]	0.727 272[−2]	−0.154 680	−0.142 220
	$3d\varepsilon f$	0.375 735[−4]	0.982 441[−2]	0.111 658[+1]	−0.163 431[+1]

TABLE II. (*Continued*).

s	μ	σ_μ^0 (Mb)	Γ_μ^s (eV)	Re (α_μ^s)	Im (α_μ^s)
$7\,^1P^\circ(3,0)_6$	$1s\varepsilon p$	0.767 036	0.664 800[−7]	0.595 484[−4]	0.174 412[−5]
	$2s\varepsilon p$	0.335 662[−1]	0.563 913[−5]	−0.261 885[−2]	−0.144 866[−3]
	$2p\varepsilon s$	0.331 193[−1]	0.768 974[−5]	0.307 929[−2]	0.159 684[−3]
	$2p\varepsilon d$	0.179 857[−1]	0.255 066[−5]	−0.187 911[−2]	0.150 867[−2]
	$3s\varepsilon p$	0.347 177[−2]	0.288 894[−3]	−0.356 842[−1]	0.461 958[−1]
	$3p\varepsilon s$	0.529 077[−2]	0.324 424[−3]	0.248 914[−1]	−0.434 894[−1]
	$3p\varepsilon d$	0.370 471[−2]	0.114 973[−3]	−0.167 651[−1]	0.314 601[−1]
	$3d\varepsilon p$	0.302 948[−2]	0.993 935[−4]	0.254 531[−1]	−0.263 744[−1]
	$3d\varepsilon f$	0.350 946[−3]	0.141 532[−4]	−0.388 668[−1]	0.118 646[−1]
$8\,^1P^\circ(-2,1)_4$	$1s\varepsilon p$	0.762 994	0.157 088[−5]	0.344 984[−3]	0.236 433[−4]
	$2s\varepsilon p$	0.344 438[−1]	0.576 592[−4]	0.158 719[−2]	−0.973 160[−2]
	$2p\varepsilon s$	0.327 048[−1]	0.929 919[−4]	0.468 422[−2]	0.119 664[−1]
	$2p\varepsilon d$	0.168 356[−1]	0.993 372[−3]	0.185 365[−1]	0.555 270[−1]
	$3s\varepsilon p$	0.380 310[−2]	0.399 195[−2]	−0.743 005[−1]	−0.235 460
	$3p\varepsilon s$	0.580 584[−2]	0.386 419[−2]	−0.681 145[−1]	−0.184 433
	$3p\varepsilon d$	0.296 316[−2]	0.327 362[−2]	0.191 656	0.165 624
	$3d\varepsilon p$	0.140 372[−2]	0.333 655[−2]	0.162 658	0.334 051
	$3d\varepsilon f$	0.125 792[−3]	0.520 011[−5]	0.449 390[−1]	−0.195 287[−1]
$9\,^1P^\circ(-1,0)_5$	$1s\varepsilon p$	0.760 982	0.147 551[−7]	0.171 003[−5]	−0.186 899[−4]
	$2s\varepsilon p$	0.347 033[−1]	0.150 476[−5]	−0.187 339[−3]	0.867 531[−3]
	$2p\varepsilon s$	0.322 815[−1]	0.186 331[−6]	−0.123 083[−4]	−0.323 583[−3]
	$2p\varepsilon d$	0.161 961[−1]	0.122 803[−4]	0.100 642[−3]	−0.370 999[−2]
	$3s\varepsilon p$	0.405 513[−2]	0.236 898[−4]	0.904 418[−2]	0.493 243[−2]
	$3p\varepsilon s$	0.601 523[−2]	0.447 735[−4]	−0.562 566[−2]	0.101 769[−1]
	$3p\varepsilon d$	0.188 772[−2]	0.260 360[−4]	−0.157 597[−1]	−0.147 859[−2]
	$3d\varepsilon p$	0.740 436[−3]	0.954 933[−4]	0.428 503[−1]	−0.225 109[−1]
	$3d\varepsilon f$	0.118 837[−3]	0.287 073[−4]	0.284 480[−1]	−0.598 259[−1]
$10\,^1P^\circ(2,1)_6$	$1s\varepsilon p$	0.765 785	0.308 266[−3]	−0.315 550[−2]	−0.228 701[−1]
	$2s\varepsilon p$	0.334 257[−1]	0.176 925[−2]	0.141 925	0.223 475
	$2p\varepsilon s$	0.315 235[−1]	0.487 845[−2]	0.324 973	0.315 174
	$2p\varepsilon d$	0.151 272[−1]	0.281 094[−2]	0.304 209	0.391 784
	$3s\varepsilon p$	0.535 619[−2]	0.306 605[−2]	0.863 681	−0.109 492
	$3p\varepsilon s$	0.900 768[−2]	0.618 282[−2]	0.925 323	−0.229 358
	$3p\varepsilon d$	0.444 269[−2]	0.433 256[−2]	0.107 991[+1]	−0.353 605
	$3d\varepsilon p$	0.224 411[−2]	0.449 873[−2]	0.145 127[+1]	−0.740 368
	$3d\varepsilon f$	0.640 852[−4]	0.123 427[−2]	0.493 558[+1]	0.106 830[+1]
$11\,^1P^\circ(1,0)_6$	$1s\varepsilon p$	0.779 212	0.553 909[−7]	0.251 279[−4]	−0.101 940[−3]
	$2s\varepsilon p$	0.282 249[−1]	0.168 599[−5]	−0.792 071[−4]	−0.304 247[−2]
	$2p\varepsilon s$	0.255 675[−1]	0.238 106[−7]	0.359 600[−3]	0.122 885[−3]
	$2p\varepsilon d$	0.113 681[−1]	0.138 376[−4]	0.107 509[−1]	0.855 408[−2]
	$3s\varepsilon p$	0.676 775[−2]	0.199 424[−3]	−0.570 191[−1]	0.363 071[−1]
	$3p\varepsilon s$	0.127 050[−1]	0.765 994[−4]	0.279 749[−1]	−0.123 421[−1]
	$3p\varepsilon d$	0.764 268[−2]	0.248 774[−3]	0.489 260[−1]	−0.515 153[−1]
	$3d\varepsilon p$	0.530 412[−2]	0.452 817[−3]	−0.666 077[−1]	0.938 177[−1]
	$3d\varepsilon f$	0.330 500[−3]	0.470 462[−3]	0.266 433	−0.386 977
$12\,^1P^\circ(0,1)_6$	$1s\varepsilon p$	0.760 946	0.816 347[−5]	−0.196 219[−4]	−0.233 054[−3]
	$2s\varepsilon p$	0.336 639[−1]	0.123 038[−3]	−0.379 447[−2]	0.205 845[−2]
	$2p\varepsilon s$	0.318 797[−1]	0.840 791[−4]	0.598 946[−4]	−0.366 655[−2]
	$2p\varepsilon d$	0.158 197[−1]	0.131 797[−2]	0.631 172[−2]	−0.196 200[−1]
	$3s\varepsilon p$	0.417 257[−2]	0.314 225[−2]	0.523 643[−1]	0.331 311[−1]
	$3p\varepsilon s$	0.732 262[−2]	0.702 493[−2]	0.472 136[−1]	0.515 974[−1]
	$3p\varepsilon d$	0.521 409[−2]	0.245 655[−2]	−0.289 902[−1]	0.395 190[−1]
	$3d\varepsilon p$	0.293 947[−2]	0.567 262[−2]	−0.849 749[−1]	−0.511 739[−1]
	$3d\varepsilon f$	0.464 522[−4]	0.592 804[−2]	0.192 830	−0.783 257

acter mixing between them and, therefore, less conservation of a given property within a series.

It can be seen from Table II, that the α_μ^s parameters are also very similar for all the resonances of the (2,1) series. As for the Fano parameters, this is not so clear for other series, although the relative signs of the real and the imaginary parts are more or less conserved. The largest α_μ^s values are for the $N=3$ channels, which explains why the resonances structures are more apparent in the corresponding cross sections.

The fact that the background cross sections σ^0 or σ_μ^0 do not decrease monotonically when the energy increases is due to the inclusion of the effect of neighboring resonances. This is rather obvious for needlelike resonances embedded in larger resonances structures that strongly contribute to the background of the formers.

Addition of the partial widths associated to the same threshold leads to the following approximate relations for each series:

$$\begin{aligned}
&(2,1)_n\ ,\ \Gamma_{N=3}\simeq 2\Gamma_{N=2}\gg\Gamma_{N=1}\ ,\\
&(0,1)_n,(-2,1)_n\ ,\ \Gamma_{N=3}\simeq 12\Gamma_{N=2}\gg\Gamma_{N=1}\ ,\\
&(3,0)_n,(1,0)_n\ ,\ \Gamma_{N=3}\gg\Gamma_{N=2}\gg\Gamma_{N=1}\ ,\\
&(-1,0)_n\ ,\ \Gamma_{N=3}\simeq 18\Gamma_{N=2}\gg\Gamma_{N=1}\ ,
\end{aligned}\tag{11}$$

in an obvious notation. In all cases, $\Gamma_{N=1}$ is negligible with respect to $\Gamma_{N=2}$ and $\Gamma_{N=3}$. $\Gamma_{N=3}$ is at least one order of magnitude larger than $\Gamma_{N=2}$, except for the (2,1) series, where they are comparable. This is in contrast with the usual situation, in which doubly excited states autoionize almost exclusively to the closest threshold. Table II also shows that there are not clearly propensity rules favoring one particular channel: partial widths associated to the same threshold do not differ appreciably between them, except for the $2p\varepsilon d$ and $3d\varepsilon f$ ones which, in some cases, are significantly smaller than the others.

Several authors have evaluated energy positions [15–20] and total widths [16–18] for the $4lnl'$ doubly excited states. Energy calculations of Herrick and Sinanoglu [16], and Robaux [20] have been performed with the truncated diagonalization method (TDM) in a basis of hydrogenic configurations. Oberoi [15] have calculated energy positions with a conventional Feshbach approach by using hydrogenic orbitals for the inner electron. In these three calculations, the Feshbach energy shift [28] has not been evaluated and convergence of the results is slow due to the use of hydrogenic orbitals. This may be the origin of the different energy ordering found by these authors for resonances that are very close in energy, when they are compared with our results or those of Ho [18]. Herrick and Sinanoglu [16] have also evaluated total widths by neglecting interchannel couplings. This may be a poor approximation in the present case, since the $3l\varepsilon l'$ channels are strongly coupled (see paper I).

In Table III we compare our calculated energies and total widths with the theoretical results of Ho [18], which are the most accurate ones reported in the literature. As for the present calculations, Ho's results include energy shifts and interchannel coupling. We have also included the experimental values of Woodruff and Samson [3], and

TABLE III. Comparison of our calculated resonant parameters with the theoretical results of Ho [18] and the experimental data of Woodruff and Samson [3] and Zubek *et al.* [5]. The latter have been converted to a.u. using the equivalence 1 a.u. = 27.211 687 eV and the ground-state energy $E_g = -2.903\,724\,38$ a.u. Numbers within parentheses indicate the uncertainty in the final figures. Resonances are labeled as in Table I. (a) Energy positions in a.u.; (b) total widths in eV.

State	This work	Ho Ref. [18]	Woodruff and Samson Ref. [3]	Zubek *et al.* Ref. [5]
		(a) Energy positions (a.u.)		
$1\,^1P^\circ(2,1)_4$	−0.194 43	−0.194 54	−0.1968(11)	−0.1947(11)
$2\,^1P^\circ(0,1)_4$	−0.178 31	−0.178 82	−0.1788(15)	−0.1797(11)
$3\,^1P^\circ(3,0)_5$	−0.168 85	−0.168 85		
$4\,^1P^\circ(2,1)_5$	−0.161 24	−0.161 27	−0.1634(11)	−0.1624(11)
$5\,^1P^\circ(1,0)_5$	−0.160 69	−0.1607		
$6\,^1P^\circ(0,1)_5$	−0.152 58	−0.1528		−0.1559(11)
$7\,^1P^\circ(3,0)_6$	−0.151 82	−0.151 84		
$8\,^1P^\circ(-2,1)_4$	−0.150 49	−0.150 59		
$9\,^1P^\circ(-1,0)_5$	−0.149 72	−0.1498		
$10\,^1P^\circ(2,1)_6$	−0.147 92		−0.1501(11)	−0.1492(11)
		(b) Widths (eV)		
$1\,^1P^\circ(2,1)_4$	0.078	0.098		0.089(8)
$2\,^1P^\circ(0,1)_4$	0.097	0.129		
$3\,^1P^\circ(3,0)_5$	0.001	0.001		
$4\,^1P^\circ(2,1)_5$	0.048	0.061		
$5\,^1P^\circ(1,0)_5$	0.002	0.003		
$6\,^1P^\circ(0,1)_5$	0.036	0.056		
$7\,^1P^\circ(3,0)_6$	0.0009	0.0004		
$8\,^1P^\circ(-2,1)_4$	0.016	0.019		
$9\,^1P^\circ(-1,0)_5$	0.0002	0.0001		

Zubek *et al.* [5]. The energy positions are in very good agreement with those of Ho. The energies reported by Zubek *et al.* [5] for the (2,1) resonances are also in reasonable agreement with the theoretical values. On the other hand, energy positions tabulated by Woodruff and Samson for this (2,1) series are probably too low. Concerning the (0,1) series, it must be taken into account that the experimental determination of the corresponding energy positions states is very difficult since, as mentioned above, the (0,1) resonances are "hidden" in the spectra (see Figs. 4 and 7). Consequently, the experimental values could be affected by large uncertainties in this case.

The autoionization widths are also in reasonable agreement with those of Ho, although ours are slightly smaller. The experimental value reported by Zubek *et al.* [5] for the first (2,1) resonance lies between both theoretical results.

Finally, Domke *et al.* [22] have determined the line profile parameter for the (2,1) resonances. Their reported value, $q_s = 0.45$, is in very good agreement with our result for the first resonance, $q_s = 0.48$.

IV. SUMMARY

In this paper we have presented extensive calculations of partial photoionization cross sections of He between the $N=3$ and 4 thresholds. We have used the L^2 method recently proposed by Martín [14], which is based on the Feshbach formalism and makes use of L^2 bases to describe both resonant and nonresonant contributions to the continuum wave functions. An appealing feature of this method is that interchannel coupling is fully accounted for by simply solving a system of linear equations. Therefore, it is well adapted to study photoionization when the number of channels is large and/or interchannel coupling is strong.

In the energy region considered in this work there are nine open channels, which are associated to the $N=1$, 2, and $N=3$ thresholds. Therefore, after ejection of one electron, the residual He^+ ion can be left in the ground or $N=2$ and 3 excited states. Our results confirm that photoionization produces mainly He^+ in a $1s$ state. However, the corresponding cross section only exhibits resonances of the (2,1) series. On the other hand, the $N=3$ cross sections, which are the smallest ones, exhibit all the resonances associated to the $4lnl'$ doubly excited states. We have also found that the $2p$ cross section dominates the $N=2$ results, and that the $3p$ cross section dominates the $N=3$ ones.

We have evaluated a complete set of resonance parameters (energy positions, total and partial widths, Fano and Starace parameters) for the first 12 doubly excited states lying in this region. The largest autoionization widths correspond to the (2,1), (0,1), and (−2,1) series. The analysis of the partial widths indicates that autoionization through the $N=3$ channels is much more important than through the $N=2$ ones, except for the (2,1) resonances for which $\Gamma_{N=2}$ is one half of $\Gamma_{N=3}$. In all cases, $\Gamma_{N=1}$ is negligible. The correlation parameter ρ_s^2 is very small for all the resonances except for the (2,1) ones, which explains why this is the only series observed in the total-cross-section spectrum. On the other hand, the Starace parameters α_μ^s associated to the $N=3$ channels have non-negligible values, thus explaining why the whole resonance structure is seen in the $N=3$ partial cross sections.

ACKNOWLEDGMENTS

This work has been partially supported by the DGICYT Project No. PB90-213 and the EEC twining program SCI*.0138.C(JR).

[1] D. W. Lindle, T. A. Ferrett, U. Becker, P. H. Kobrin, C. M. Truesdale, H. G. Kerkhoff, and D. A. Shirley, Phys. Rev. A **31**, 714 (1985).
[2] P. R. Woodruff and J. A. R. Samson, Phys. Rev. Lett. **45**, 110 (1980).
[3] P. R. Woodruff and J. A. R. Samson, Phys. Rev. A **25**, 848 (1982).
[4] D. W. Lindle, T. A. Ferrett, P. A. Heimann, and D. A. Shirley, Phys. Rev. A **36**, 2112 (1987).
[5] M. Zubek, G. C. King, P. M. Rutter, and F. H. Read, J. Phys. B **22**, 3411 (1989).
[6] S. M. Burkov, N. A. Letyaev, S. I. Strakhova, and T. M. Zajac, J. Phys. B **21**, 1195 (1988).
[7] S. Salomonson, S. L. Carter, and H. P. Kelly, J. Phys. B **18**, L149 (1985).
[8] M. A. Hayes and M. P. Scott, J. Phys. B **21**, 1499 (1988).
[9] S. Salomonson, S. L. Carter, and H. P. Kelly, Phys. Rev. A **39**, 5111 (1989).
[10] R. Moccia and P. Spizzo, Phys. Rev. A **43**, 2199 (1991).
[11] I. Sánchez and F. Martín, Phys. Rev. A **44**, 13 (1991).
[12] I. Sánchez and F. Martín, Phys. Rev. A **44**, 7318 (1991).
[13] I. Sánchez and F. Martín, Phys. Rev. A **45**, 4468 (1992).
[14] F. Martín, Phys. Rev. A **48**, 331 (1993).
[15] R. S. Oberoi, J. Phys. B **5**, 1120 (1972).
[16] D. R. Herrick and O. Sinanoglu, Phys. Rev. A **11**, 97 (1975).
[17] Y. K. Ho, Phys. Lett. **79A**, 44 (1980).
[18] Y. K. Ho, J. Phys. B **15**, L691 (1982).
[19] Y. Komninos and C. A. Nicolaides, J. Phys. B **19**, 1701 (1986).
[20] O. Robaux, J. Phys. B **20**, 2347 (1987).
[21] P. A. Heimann, U. Becker, H. G. Kerkhoff, B. Langer, D. Szostak, R. Wehlitz, D. W. Lindle, T. A. Ferrett, and D. A. Shirley, Phys. Rev. A **34**, 3782 (1986).
[22] M. Domke, C. Xue, A. Puschmann, T. Mandel, E. Hudson, D. A. Shirley, G. Kaindl, C. H. Green, H. R. Sadeghpour, and H. Petersen, Phys. Rev. Lett. **66**, 1306 (1991).
[23] Y. Hahn, T. F. O'Malley, and L. Spruch, Phys. Rev. **128**, 932 (1962).
[24] F. Martín, O. Mó, A. Riera, and M. Yáñez, Europhys. Lett. **4**, 799 (1987); J. Chem. Phys. **87**, 6635 (1987).
[25] A. Macías, F. Martín, A. Riera, and M. Yáñez, Phys. Rev. A **36**, 4179 (1987); Int. J. Quantum Chem. **33**, 279 (1988).
[26] U. Fano, Phys. Rev. **124**, 1866 (1961); U. Fano and J. W. Cooper, **137**, A1364 (1965).
[27] A. F. Starace, Phys. Rev. A **16**, 231 (1977).
[28] H. Feshbach, Ann. Phys. (N.Y.) **19**, 287 (1962).